International Journal of Nanomedicine

Dovepress
open access to scientific and medical research

Open Access Full Text Article

ORIGINAL RESEARCH

Fabricating polydopamine-coated $MoSe_2$-wrapped hollow mesoporous silica nanoplatform for controlled drug release and chemo-photothermal therapy

This article was published in the following Dove Press journal:
International Journal of Nanomedicine

Song Chai[1,*]
Shifeng Kan[1,*]
Ran Sun[1]
Ruijuan Zhou[1]
Yi Sun[2]
Wenhua Chen[1]
Bo Yu[1,3]

[1]Department of Rehabilitation, Shanghai General Hospital, Shanghai Jiaotong University, Shanghai 200080, China; [2]Department of Rehabilitation, Shanghai Sunshine Rehabilitation Center, Yangzhi Affiliated Rehabilitation Hospital of Tongji University, Shanghai 201209, China; [3]Department of Rehabilitation Therapy, School of International Medical Technology, Shanghai Sanda University, Shanghai 201209, China

*These authors contributed equally to this work

Background: Integration of several types of therapeutic agents into one nanoplatform to enhance treatment efficacy is being more widely used for cancer therapy.

Methods: Herein, a biocompatible polydopamine (PDA)-coated $MoSe_2$-wrapped doxorubicin (DOX)-loaded hollow mesoporous silica nanoparticles (HMSNs) nanoplatform (PM@HMSNs-DOX) was fabricated for dual-sensitive drug release and chemo-photothermal therapy for enhancing the therapeutic effects on breast cancer. The HMSNs were obtained by a "structural difference-based selective etching" strategy and served as the drug carrier, exhibiting a high DOX loading capacity of 427 mg/g HMSNs-NH_2, and then wrapped with PDA-coated $MoSe_2$ layer to form PM@HMSNs-DOX. Various techniques proved the successful fabrication of the nanocomposites.

Results: The formed PM@HMSNs-DOX nanocomposites exhibited good biocompatibility, good stability, and super-additive photothermal conversion efficiency due to the cooperation of $MoSe_2$ and PDA. Simultaneously, the pH/near-infrared-responsive drug release profile was observed, which could enhance the synergistic therapeutic anticancer effect. The antitumor effects of PM@HMSNs-DOX were evaluated both in vitro and in vivo, demonstrating that the synergistic therapeutic efficacy was significantly superior to any monotherapy. Also, in vivo pharmacokinetics studies showed that PM@HMSNs-DOX had a much longer circulation time than free DOX. In addition, in vitro and in vivo toxicity studies certified that PM@HMSNs are suitable as biocompatible agents.

Conclusion: Our nanoplatform loaded with DOX displays pH/near-infrared-induced chemotherapy and excellent photothermal therapy, which hold great potential for cancer treatment.

Keywords: hollow mesoporous silica nanoparticles, $MoSe_2$, polydopamine, chemo-photothermal therapy

Introduction

Cancer has been recognized as one of the deadliest diseases worldwide for decades and remains a serious health concern.[1,2] Despite tremendous progress of current medicines for cancer therapy, only limited success has been realized because the tumors are complex, diverse, and heterogeneous.[3] Therefore, a single treatment modality (chemotherapy, radiation therapy, etc) is far from achieving the ideal tumor suppressor effect. It is ineffective in preventing cancer metastasis in both clinical research and laboratory studies.[4] To overcome these obstacles, synergistic therapy, which employs the integration of therapeutic methodologies to improve treatment efficacy, has been proposed as a flexible approach.[5] More importantly,

Correspondence: Bo Yu; Wenhua Chen
Department of Rehabilitation, Shanghai General Hospital, Shanghai Jiaotong University, No 100, Haining Road, Shanghai 200080, China
Tel +86 21 6 324 0090
Email ybsykf@163.com; chen.wh@163.com

submit your manuscript | www.dovepress.com
Dovepress
http://dx.doi.org/10.2147/IJN.S181681

nanotechnology empowers these therapeutic modalities by assembling various therapeutic elements into one nanoplatform, thus forming multifunctional nanomaterials for achieving a multimodal synergistic therapy.[6] In this regard, a variety of synergistic nanoplatforms has been proposed, such as chemo-photothermal therapy (PTT),[7,8] chemo-photodynamic therapy (PDT),[9,10] chemotherapy-immunotherapy,[11] PTT/PDT,[12,13] and so on. Among these, the combination of PTT and chemotherapy is attracting more attention due to the enhancement of anticancer efficacy in cancer treatment.

To construct a chemo-PTT system, one prerequisite is to obtain a biocompatible nanocarrier for drug loading and efficient photothermal conversion nanomaterials coating for inducing mild hyperthermia. To date, different types of nanomaterials (both organic and inorganic) have been studied for cancer synergistic chemo-PTT, including synthetic polymers,[14] carbon-based nanostructures,[15] mesoporous silica,[16] and nanoscale metal-organic frameworks.[17] Among the explored drug carriers, mesoporous silica nanoparticles (MSNs) are becoming well-known for nanomedicine due to their high surface area, stable porous structure, noninvasive nature, excellent biocompatibility, and easy surface functionalization.[18] As a specific member of the MSNs-based nanofamily, hollow MSNs (HMSNs) possess all the advantages of MSNs and also contain a unique hollow architecture, which can act as large reservoirs for cargo loading and reduce the intrusion of impurities into bodies.[19] Up to now, various types of HMSNs-based chemo-PTT systems have been developed. For instance, Fang et al constructed a nanoplatform based on Pd nanosheet-covered HMSNs for chemo-PTT.[20] Hu et al designed folic acid-conjugated hollow mesoporous silica/CuS nanocomposites for targeted chemo-PTT of cancer.[21] However, designing a smart and controllable gatekeeper for the HMSNs in the delivery process to realize a more selective synergistic therapy is still becoming a key challenge.

On the other hand, for cancer chemo-PTT therapy, an ideal photothermal conversion agent for inducing mild hyperthermia is essential. A series of near-infrared (NIR) light absorbing inorganic nanomaterials including gold nanostructures,[22] carbon nanomaterials (carbon nanotube, graphene oxide),[23] black phosphorus,[24] copper sulfide nanoparticles,[25] as well as organic nanoparticles such as NIR dyes and polydopamine (PDA),[26,27] have been extensively studied for PTT ablation of cancer cells in vitro and in vivo. Recently, burgeoning two-dimensional (2D) nanomaterials, transition metal dichalcogenides (MoS_2, WS_2, WSe_2, $MoSe_2$, etc.) have drawn tremendous attention due to their unique properties as well as their applications in the biomedical field.[28–30] Until now, only few studies have reported using these 2D nanomaterials as photothermal agents and NIR light-responsive gatekeepers simultaneously in MSNs-based drug delivery systems. Zhao et al developed a method for synthesizing transferrin-decorated, stimuli-responsive MoS_2-capped HMSNs as a dual-functional drug delivery system.[31] Also, Wu et al designed a multifunctional platform based on a functionalized MoS_2 nanosheet-wrapped periodic mesoporous organosilica nanoparticles nanoplatform for both targeting drug delivery and synergistic chemo-PTT.[32] Despite the general progress, chemical instability in vitro and in vivo for biomedical applications still has been a critical challenge. In this case, PDA was introduced to overcome the stability of 2D nanomaterials due to unique features such as good biocompatibility, biodegradability, and also it can form an adhesive layer onto the surface of various types of materials.[33,34] More importantly, the strong NIR absorption of PDA makes it suitable for use as an ideal photothermal agent for PTT.[35] Thanks to the versatile property of PDA, we believe that PDA coating can improve biocompatibility and enhance the PTT efficiency of semiconductor nanomaterials simultaneously. Moreover, the utilization of these PDA-coated 2D nanomaterials as smart gatekeeper in HMSNs-based drug delivery systems has not been reported to the best of our knowledge.

Herein, a biocompatible PDA-coated $MoSe_2$ sheets-wrapped doxorubicin (DOX)-loaded HMSNs nanoplatform (PM@HMSNs-DOX) was fabricated for pH/NIR-sensitive drug release and chemo-PTT for enhancing the therapeutic effects on breast cancer (Figure 1). HMSNs serve as a carrier for drug loading. The PDA-coated $MoSe_2$ sheets were not only used as a gatekeeper for preventing the burst release of drug molecules in blood circulation but also as potential enhanced photothermal agents due to the cooperation of PDA and $MoSe_2$ nanosheets. In case of being present at weak acidic tumor tissue/cells (pH <6.8),[36] the loaded DOX could be on-demand released due to the pH-induced breakage of PDA and high local temperature under laser irradiation triggered the vibration of the $MoSe_2$ nanosheets. Moreover, PM@HMSNs-DOX exhibits satisfactory synergistic chemotherapy and PTT effect in breast cancer in vitro and in vivo. Therefore, these PM@HMSNs-DOX nanoparticles with biocompatibility, pH/NIR-responsive drug release, enhanced photothermal conversion efficiency, and excellent chemo-PTT properties are promising agents for cancer treatment.

Experimental methods

Materials

Tetraethyl orthosilicate (TEOS), ethanol, Na_2CO_3, ammonia solution (25%), 3-aminopropyltrimethoxysilane (APTES),

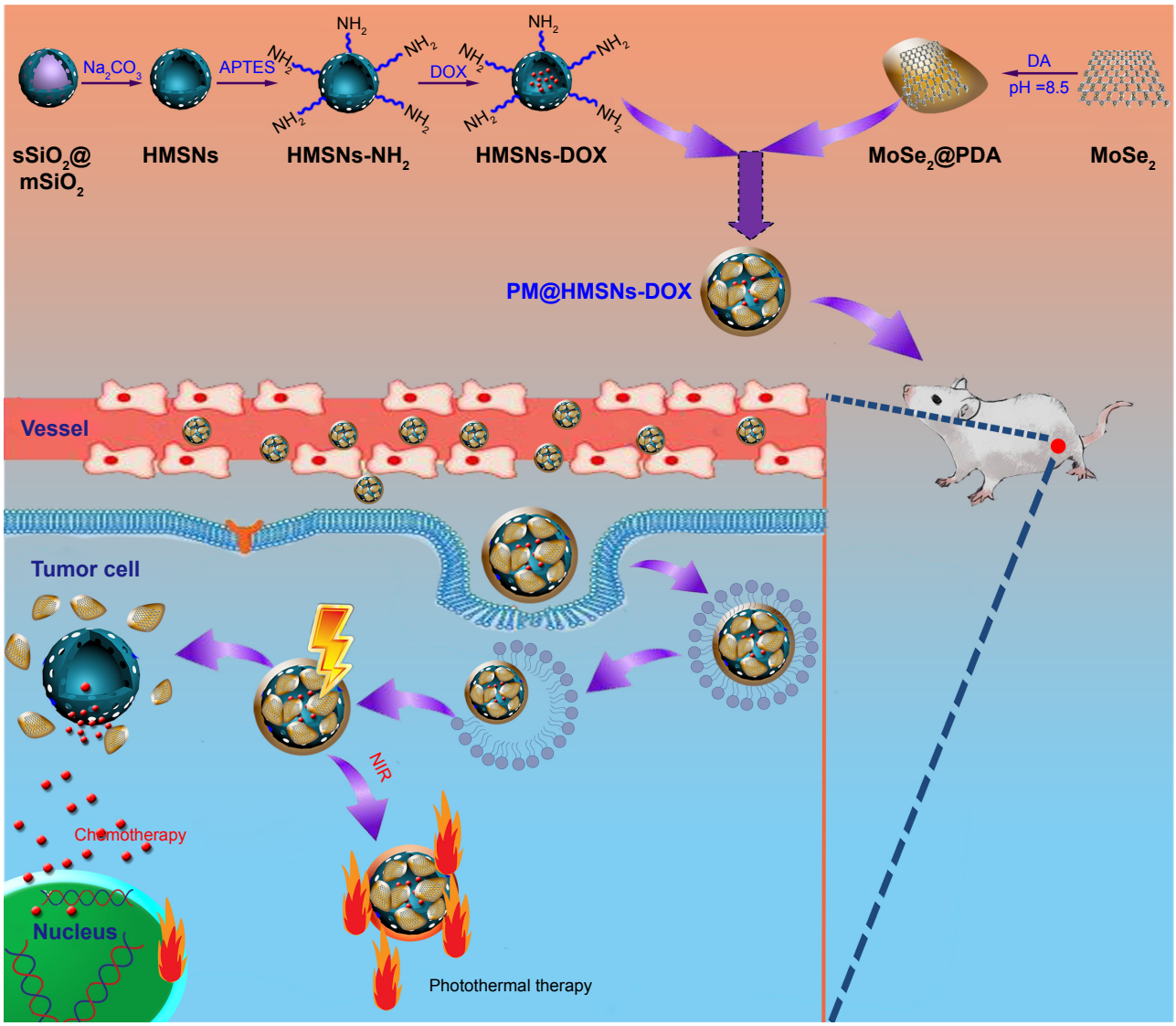

Figure 1 Schematic representation of the construction of PM@HMSNs-DOX for pH/NIR-responsive drug release and chemo-photothermal therapy.
Abbreviations: $sSiO_2@mSiO_2$, solid silica core/mesoporous silica shell; HMSNs, hollow mesoporous silica nanoparticles; SiO_2, silicon dioxide; APTES, 3-aminopropyltrimethoxysilane; DOX, doxorubicin; DA, dopamine; PDA, polydopamine; PM, polydopamine-coated $MoSe_2$; NIR, near-infrared.

$NaBH_4$, $Na_2MoO_4{\cdot}2H_2O$, and isopropanol were obtained from Sinopharm Chemical Reagent Co., Ltd. (Shanghai, China). Dopamine hydrochloride, DOX hydrochloride, calcein acetoxymethyl ester (calcein AM), and propidium iodide (PI) were purchased from Aladdin Reagent Co. (Shanghai, China). Octadecyltrimethoxysilane (C_{18}TMS), selenide (Se) power, dimethyl sulfoxide, and DAPI were purchased from Sigma-Aldrich (St Louis, MO, USA). DMEM, cell counting kit-8 (CCK-8), antibiotics (penicillin/streptomycin), tris(hydroxymethyl)aminomethane (Tris) buffer, FBS, and PBS were bought from Thermo Fisher Scientific, Waltham, MA, USA. All reagents were used without further purification. Deionized water was used in all experiments (Milli-Q, 18.2 MΩ cm; Merck Millipore, Billerica, MA, USA).

Synthesis of HMSNs and amino functionalization

For the synthesis of HMSNs, a modified procedure was used as previously described and a structural difference-based selective etching strategy was employed to remove the solid silica core.[37] Briefly, ethanol (71.4 mL), H_2O (10 mL), and ammonia solution (3.14 mL) were mixed under stirring at 30°C for 30 minutes. Then, TEOS (6 mL) was rapidly added and stirred for another 1 hour. Thereafter, 5 mL of TEOS and 2 mL of C_{18}TMS were pre-blended and introduced into the above solution. Then, the mixture was allowed to react at 55°C for 1 hour to form solid silica core/mesoporous silica shell ($sSiO_2@mSiO_2$) nanoparticles. The

as-prepared $sSiO_2$@$mSiO_2$ nanoparticle was divided into eight pieces on average and dispersed in Na_2CO_3 (0.6 M, 40 mL) at 80°C for 1 hour. The HMSNs were collected by centrifugation, washed with ethanol several times, followed by drying at 100°C and calcining at 550°C for 6 hours to remove the surfactant.

For the synthesis of HMSNs-NH_2, HMSNs (100 mg) were dispersed in 20 mL anhydrous toluene and 100 μL of APTES was added and refluxed at 120°C for 12 hours. After centrifugation at 11,000 rpm for 10 minutes and washing with ethanol for three times, the final product was collected for subsequent use.

Synthesis of $MoSe_2$@PDA

The $MoSe_2$ nanosheets were synthesized according to previously published literature.[38] Briefly, the Se powder (200 mg) was added into $NaBH_4$ aqueous solution (5 mM, 10 mL) under stirring for 15 minutes. Then, $Na_2MoO_4 \cdot 2H_2O$ (0.5 g, 0.02 g/mL) was added into the reaction solution and vigorously stirred for 1 hour. Subsequently, the mixture was transferred into a Teflon-lined autoclave (50 mL) and maintained at 180°C for 12 hours. The product was obtained by centrifugation, and then washed with water several times and stored at 4°C for further use.

For PDA coating, the obtained $MoSe_2$ nanosheets were dispersed in 40 mL of Tris buffer solution (10 mM, pH 8.5) containing dopamine (0.4 mM) and vigorously stirred overnight at room temperature. Afterward, the product was collected by centrifugation, washed with distilled water several times, and designated as PDA@$MoSe_2$.

Preparation of $MoSe_2$@PDA-coated DOX-loaded HMSNs (HMSNs-DOX)

HMSNs–NH_2 nanoparticles (10 mg) and 4 mg of DOX were mixed in 3 mL of ultrapure water, and stirred for 24 hours under dark conditions. Then, HMSNs-DOX were collected by centrifugation and washed with deionized water to remove the excess DOX. The loading capacity was evaluated according to the changes of DOX concentration before and after drug loading using an ultraviolet–visible (UV–vis) spectrometer at a wavelength of 490 nm. For $MoSe_2$@PDA wrapping, 10 mg of $MoSe_2$@PDA was resuspended in 5 mL of water under sonication for several minutes to form the uniform dispersion. Then, the $MoSe_2$@PDA dispersion was added into the above HMSNs-DOX solution under ultrasonication to get a homogeneous solution and stirred for 2 hours. After that, the products were designated as PM@HMSNs-DOX, which was collected by centrifugation, washed with water, and dried via lyophilization. PM@HMSNs were also prepared by using the same procedure but without DOX loading.

Characterization of the nanoparticles

The morphology and structure of the nanoparticles were observed using transmission electron microscopy (TEM, JEM-2100; JEOL Ltd., Tokyo, Japan). The particle size and ζ potential measurements of the prepared nanoparticles were carried out on a Zetasizer Nano ZS apparatus (Malvern Instruments Ltd., Malvern, UK). N_2 adsorption/desorption isotherms were recorded at −196°C using an automated absorption analyzer (ASAP 2020; Micromeritics Instruments Corporation, Norcross, GA, USA). The surface areas and pore size distributions were determined by Brunauer−Emmett−Teller (BET) and Barrett−Joyner−Halenda (BJH) methods, respectively. Fourier transform infrared (FT-IR) spectra were recorded on a Nexus 670 spectrometer by KBr disc technique (Thermo Fisher Scientific). The content of Si element was analyzed by a Leeman Prodigy inductively coupled plasma-atomic emission spectroscopy (ICP-AES) system (Thermo E IRIS Duo; Thermo Fisher Scientific). The UV–vis–NIR absorption spectra were recorded using a Shimadzu UV-3600 spectrophotometer (Shimadzu Corporation, Kyoto, Japan).

Photothermal effect measurement

An NIR laser (808 nm; SFOLT Co., Ltd., Shanghai, China) was used to measure the photothermal effect of nanoparticles and perform the following in vitro/vivo PTT experiments. Changes of the solution were monitored by a thermocouple thermometer (DT-8891E; Shenzhen Everbest Machinery Industry Co., Ltd., China). To determine the photothermal effect of PM@HMSNs-DOX, 0.5 mL of PBS, PM@HMSNs-DOX with different concentrations (25, 50, 100, 150, 200 μg/mL) were subjected to NIR irradiation at 1.0 W/cm^2 for 5 minutes. Meanwhile, 0.5 mL of the PM@HMSNs-DOX sample at a concentration of 100 μg/mL was irradiated by NIR laser for 5 minutes with different laser powers. To investigate the photostability of PM@HMSNs, the samples were irradiated with five laser on–off cycles for temperature monitoring to detect the thermal stability of the materials. Finally, the photothermal conversion efficiency (η) was calculated according to a previous study.[39]

In vitro drug release profiles

In vitro DOX release profile of PM@HMSNs-DOX was determined by the dialysis method at different pH values of 7.4 and 5.5 with or without 808 nm NIR laser irradiation.

In brief, the PM@HMSNs-DOX nanoparticles were dispersed in the buffer solution (pH 6.0 and 7.4). Then, the dispersion was transferred into a dialysis bag (molecular weight cutoff =3,500 Da) with 20 mL release medium of PBS (pH 7.4) and shaken in a 37°C thermostatic shaking bed (MaxQ 420 HP; Thermo Fisher Scientific) at 100 rpm. For the NIR irradiation group, the samples were exposed to laser irradiation (808 nm, 1.0 W/cm^2) for 10 minutes. At designated time intervals, 1 mL of the release buffer was collected and replaced with equal volumes of fresh buffer for further release. The amount of released DOX in the buffer was determined by the UV–vis spectra at 480 nm.

The release kinetics of DOX were analyzed by an exponential equation based on Ritger–Peppas equation as follows:

$$\ln M_t/M_\infty = n \ln t + \ln k$$

where M_t and M_∞ are the amounts of drug released at time t and equilibrium time, respectively. k is the kinetic constant and n is an exponent characterizing the drug release mechanism.

In vitro cellular uptake

MDA-MB-231 cells were cultured in DMEM supplemented with 10% (v/v) FBS, antibiotic (100 U/mL penicillin and 100 μg/mL streptomycin) under a humidified atmosphere with 5% CO_2 atmosphere at 37°C.

The cellular uptake and intracellular distribution of PM@HMSNs-DOX in MDA-MB-231 cells were observed using confocal laser scanning microscopy (CLSM, Olympus FV 1000; Olympus Corporation, Tokyo, Japan). Briefly, MDA-MB-231 cells were seeded and cultured at a density of 1×10^5 cells/well in 24-well plates. The cells were further treated with free DOX or PM@HMSNs-DOX (equivalent to 5 μg/mL of DOX) and incubated for 4 hours. Meanwhile, for the laser irradiation group, cells were irradiated by 808 nm laser (1.0 W/cm^2) for 5 minutes after 2 hours incubation. Subsequently, the cells were washed with PBS, fixed with paraformaldehyde, and stained with DAPI for another 20 minutes. After that, the cells were washed with cold PBS three times and directly observed by CLSM. Subsequently, the cells were collected and dissolved by nitric acid. Then, the transparent solution was directly subjected to ICP-AES to measure the Si concentration.

Flow cytometry measurements were carried out to evaluate further quantitatively the cellular uptake amount of PM@HMSNs-DOX. MDA-MB-231 cells were seeded at a density of 1×10^5 cells/well in 6-well plates and cultured for 24 hours. Then, the cells were treated with free DOX or PM@HMSNs-DOX (equivalent to 5 μg/mL of DOX) and followed a similar process as the CLSM experiment. After that, the cells were harvested by trypsinization and the cell pellet was suspended in PBS and analyzed for DOX fluorescence intensity with a flow cytometer (BD Biosciences, San Jose, CA, USA).

In vitro cytotoxicity

The biocompatibility and cytotoxicity of the nanoparticles against MDA-MB-231 cells were evaluated by the CCK-8 test in vitro. Typically, MDA-MB-231 cells were seeded in 96-well plates with a density of 1×10^4 cells/well. After incubation for 24 hours, the cells were either incubated with different concentrations of PM@HMSNs nanocomposites (0–500 μg/mL) for the biocompatibility assay or exposed to free DOX, PDA@HMSNs-DOX, and PM@HMSNs-DOX with different DOX concentrations for the cytotoxicity assay. For the chemo-photothermal group, the cells were irradiated with 808 nm NIR laser at 1.0 W/cm^2 for 5 minutes. Then, the cells were washed with PBS and 100 μL of CCK-8 solution (0.5 mg/mL) was added to each well for another 4 hours. After that, cell viability was assessed by the absorbance at 450 nm on a microplate reader.

Furthermore, cell live/dead assays were performed to evaluate the efficiency of the synergistic therapy. Briefly, MDA-MB-231 cells were seeded into a 24-well plate. Subsequently, the cells were treated with PBS, free DOX, PM@HMSNs-DOX only, PM@HMSNs, PDA@HMSNs-DOX, and PM@HMSNs-DOX with laser irradiation (1.0 W/cm^2, 5 minutes), respectively. Note that free DOX and PM@HMSNs-DOX had the same concentration of DOX. Then, the cells were stained with calcein AM (2 μM) and PI (8 μM) for 40 minutes, and examined by a fluorescence microscope to observe their live/dead status.

Animals and tumor model

BALB/c nude female mice and Sprague Dawley (SD) rats were bought from SIPPR-BK Laboratory Animal Co., Ltd. (Shanghai, China) and used for the animal experiments directly. All animal experiments were approved by the Shanghai Jiaotong University Animal Care and Use Committee and performed in accordance with guidelines and regulations of the National Ministry of Health. In order to establish a xenografted mouse tumor model, MDA-MB-231 cells (1.5×10^7 cells) were subcutaneously injected in the scapular region of the mice.

In vivo antitumor efficacy

To evaluate the in vivo antitumor efficacy of the nanoplatform, tumor bearing mice were randomly divided into six groups (n=4) when the tumor volume grew to about 100 mm^3 and each mouse was intravenously injected with 200 μL of the various agents to evaluate the different treatments: namely, 1) saline, 2) free DOX (7.5 mg/kg), 3) PM@HMSNs with laser irradiation (1.0 W/cm^2, 10 minutes), 4) PM@HMSNs-DOX (7.5 mg/kg), 5) PDA@HMSNs-DOX (7.5 mg/kg) with laser irradiation (1.0 W/cm^2, 10 minutes), and 6) PM@HMSNs-DOX (7.5 mg/kg) with laser irradiation (1.0 W/cm^2, 10 minutes). The saline group was used as a negative control. All treatments were performed on the first, fourth, and seventh days. The body weight and tumor size were measured every 2 days and the tumor volume was calculated by the equation: $V=L\times W^2/2$, where V is the tumor volume, L is the tumor length, and W is the tumor width. When the treatment was fulfilled, the mice were euthanized and the tumors were excised, weighed, and photographed by a digital camera.

Histological staining

When the mice were sacrificed, fresh tumor tissues in different groups and the major organs (heart, liver, spleen, lung, and kidney) were collected. Then, the tissues were fixed in 4% neutral buffered formalin, and processed routinely into paraffin for the H&E assay. Finally, the sections were directly observed by an inverted fluorescence microscope (IX 70; Olympus Corporation).

In vivo pharmacokinetics assay and biodistribution analysis

To evaluate the pharmacokinetic behavior of PM@HMSNs-DOX nanoparticles, free DOX or PM@HMSNs-DOX was administrated into SD rats at a dose of 10 mg DOX equivalent/kg via the tail vein. At different time points, ~20 μL of blood was withdrawn using a heparinized tube. All the blood samples were lysed and extracted. After centrifugation to obtain the supernatant, the DOX level was determined by fluorescence measurement.

For the biodistribution study, MDA-MB-231 tumor bearing mice (n=3) were intravenously injected with PM@HMSNs-DOX at a DOX dosage of 10 mg/kg. Subsequently, the mice were sacrificed at 24 hours postinjection for extraction of the heart, liver, spleen, lung, kidney, and tumor, and then homogenized in 0.5 mL of lysis buffer. All the tissue lysate (200 μL) was mixed with Triton X-100 (10%, 100 mL). After extraction, centrifugation, the amount of DOX was quantified by fluorescence measurement.

Statistical analysis

At least three parallel trials were performed for all experiments. Statistical analysis was conducted using one-way ANOVA and Student's test. The criteria of statistical significance were $*P<0.05$, $**P<0.01$, and $***P<0.001$.

Results and discussion

Synthesis and characterization of PM@HMSNs-DOX nanoparticles

Fabrication of the multifunctional nanoplatform based on PDA-coated $MoSe_2$-wrapped HMSNs-DOX is described in Figure 1. The HMSNs were obtained via a sol–gel process by using TEOS and C_{18}TMS as a structure directing agent in the mixture of H_2O/ethanol/ammonia solution, followed by the "structural difference-based selective etching" strategy with Na_2CO_3.[37] Then, amino groups were introduced onto the pore outlet of HMSNs by using coupling agent APTES in toluene.[40] Next, the HMSNs-NH_2 nanoparticles were used as drug carrier to load anticancer drug DOX molecules. Meanwhile, the $MoSe_2$ nanosheets were prepared by a hydrothermal method and coated with PDA under alkaline conditions to form the PDA@$MoSe_2$.[38] Afterward, HMSNs-DOX was wrapped by PDA@$MoSe_2$, resulting in the formation of the PM@HMSNs-DOX nanoparticles. The cooperation of $MoSe_2$ nanosheets and the PDA layer on the surface of HMSNs-DOX was to prevent drug leakage from the HMSNs during blood circulation as well as to act as the photothermal agent for enhanced PTT. For intuitive observation of the surface morphology of $MoSe_2$@PDA nanoparticle and PM@HMSNs, TEM was carried out to characterize the as-prepared nanoparticles (Figure 2). On the basis of the TEM observation, the HMSNs were monodisperse and had an average diameter of 204 nm with uniform hollow structure (Figure 2B). Meanwhile, it can be observed that the synthesized $MoSe_2$@PDA nanocomposites have a core−shell nanostructure with an inner $MoSe_2$ core and outer PDA shell (Figure 2C). After the electrostatic adhesion of $MoSe_2$@PDA on HMSNs, PM@HMSNs was prepared and TEM shows an obvious clear layer on the periphery of the HMSNs particles, which indicated the $MoSe_2$@PDA coating on the HMSNs surface (Figure 2D). It should be noted that the diameter of PM@HMSNs was slightly larger than that of HMSNs. Dynamic light scattering (DLS) analysis (Figure 3A) shows that the hydrodynamic sizes of PM@HMSNs (294 nm) were slightly bigger than that of HMSNs-NH_2 (265 nm), which could be deemed as evidence of the successful coating of $MoSe_2$@PDA and also as consistent with the TEM images.

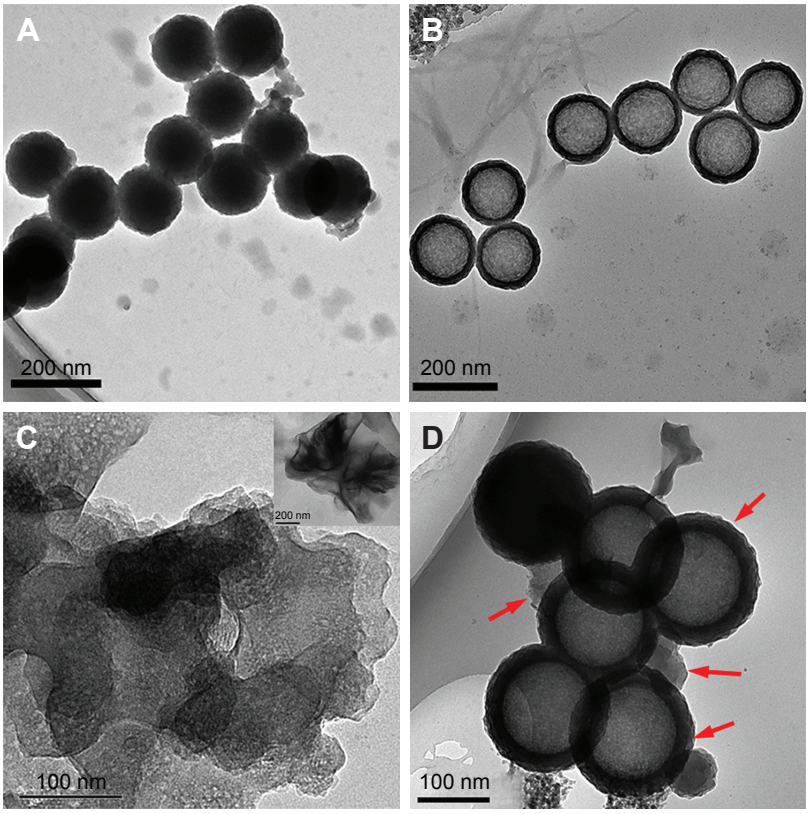

Figure 2 TEM images of PM@HMSNs.
Notes: TEM images of $sSiO_2$@$mSiO_2$ (**A**), HMSNs (**B**), polydopamine-coated $MoSe_2$ (**C**), and PM@HMSNs (**D**). Inset in (**C**) is the TEM image of $MoSe_2$ nanosheets.
Abbreviations: TEM, transmission electron microscopy; PM, polydopamine-coated $MoSe_2$; HMSNs, hollow mesoporous silica nanoparticles; $sSiO_2$@$mSiO_2$, solid silica core/mesoporous silica shell.

In addition, the N_2 adsorption–desorption measurements and pore size distribution were analyzed to investigate the mesoporous features of HMSNs-NH_2 and PM@HMSNs. As shown in Figure 3B and C, HMSNs-NH_2 exhibited a typical type IV isotherm, suggesting mesoporous structures.[41] The BET surface area and pore size estimated by the BJH method were calculated to be 779.94 m^2/g and 3.43 nm, respectively. This feature enables it to be used as an ideal drug carrier. After coating with $MoSe_2$@PDA, PM@HMSNs presented a significant decrease in the specific surface area (141.77 m^2/g) and pore size (1.45 nm). These results demonstrate that $MoSe_2$@PDA could serve as a capping agent to seal the pore to prevent pre-release of the drug.

In this case, DOX was chosen to be the anticancer model drug, which was loaded on HMSNs-NH_2. Then, HMSNs-DOX was mixed with $MoSe_2$@PDA under ultrasonication for a few minutes and stirred for 2 hours to form the $MoSe_2$@PDA-wrapped HMSNs-DOX nanoplatform (PM@HMSNs-DOX). The characteristic absorption peak of DOX at 480 nm was observed in the spectrum of HMSNs-DOX, which indicates the successful loading of DOX. The loading efficiency of HMSNs-NH_2 was measured to be about 427 mg of DOX/g of HMSNs-NH_2 with a high drug loading efficiency of 93.5% (Figure S1). After $MoSe_2$@PDA modification, the UV–vis absorption spectrum of the PM@HMSNs-DOX shows a peak at 214 nm, demonstrating the successful coating of $MoSe_2$@PDA onto the HMSNs-DOX (Figure 3D). More importantly, PM@HMSNs-DOX reveals strong absorbance in the NIR region, while HMSNs-DOX shows no absorbance in that region, suggesting that PM@HMSNs-DOX has the potential to achieve photoconversion for PTT. Also, the FT-IR absorption shows N–H scissoring at 1,485 cm^{-1} and C–O stretching at 1,270 cm^{-1}, which are the characteristic absorption of the coated $MoSe_2$@PDA (Figure 3E). To further confirm the formation of PM@HMSNs-DOX, the hydrodynamic sizes and zeta potentials of different formulations were measured. The DLS hydrodynamic diameter of PM@HMSNs-DOX is about 306 nm, which was slightly greater than that of HMSNs-NH_2 (265 nm), which was in agreement with the result of TEM and together verified that the $MoSe_2$@PDA layer was successfully coated

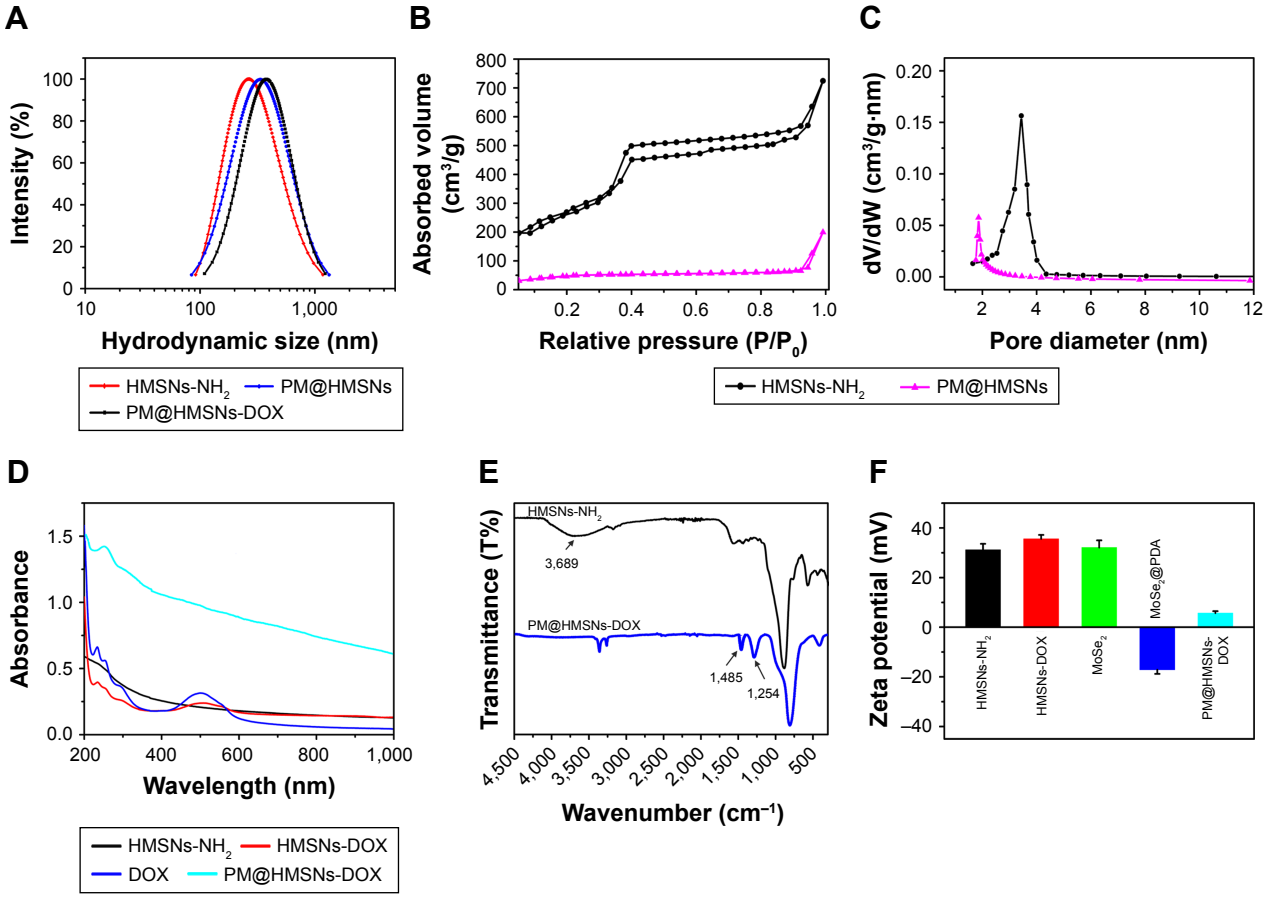

Figure 3 (**A**) Hydrodynamic diameters of HMSNs-NH_2, PM@HMSNs, and PM@HMSNs-DOX. (**B**) N_2 adsorption/desorption isotherms and (**C**) corresponding pore size distribution curve of HMSNs-NH_2 and PM@HMSNs. (**D**) UV–vis spectrum of HMSNs-NH_2, HMSNs-DOX, free DOX, and PM@HMSNs-DOX aqueous dispersion. (**E**) FT-IR spectra of HMSNs-NH_2 and PM@HMSNs-DOX. (**F**) Zeta potentials of different nanoparticles.

Abbreviations: HMSNs, hollow mesoporous silica nanoparticles; PM, polydopamine-coated $MoSe_2$; DOX, doxorubicin; UV–vis, ultraviolet–visible; FT-IR, Fourier transform infrared spectroscopy.

onto HMSNs. Meanwhile, the DLS size of the as-prepared PM@HMSNs-DOX remained nearly unchanged in different aqueous media after 1 week (Figure S2), suggesting good stability. Furthermore, the stepwise prepared HMSNs-NH_2, HMSNs-DOX, $MoSe_2$, $MoSe_2$@PDA, and PM@HMSNs-DOX were characterized by zeta potential measurements (Figure 3F). The as-prepared HMSNs-NH_2 showed a positive potential of +31.2 mV. After DOX loading, the zeta potential turned more positive to +35.6 mV because of the highly positively charged amino groups on DOX. In addition, the mean zeta potentials of $MoSe_2$ and $MoSe_2$@PDA are 32.1 and −17.2 mV, respectively. For the PM@HMSNs-DOX, the zeta potential decreased to 5.4 mV. This change in zeta potential value could be attributed to the deprotonation of the phenolic hydroxyl groups of PDA at neutral pH.[42] These results further demonstrated the successful loading of DOX and the wrapping of $MoSe_2$@PDA on HMSNs.

Photothermal performance of PM@HMSNs-DOX

Because of the strong NIR absorption of $MoSe_2$@PDA, the photothermal effect of PM@HMSNs-DOX was evaluated. Different concentrations of PM@HMSNs-DOX aqueous dispersions (50–200 μg/mL) were exposed to irradiation by NIR laser (808 nm, 1.0 W/cm^2) for 5 minutes, and 100 μg/mL of PM@HMSNs-DOX were exposed to laser irradiation with different power densities ranging from 0.5 to 1.2 W/cm^2. As shown in Figure 4A, the temperature of the dispersions at a concentration of 100 μg/mL increased from 25.2°C to 53.2°C under 5-minute NIR irradiation, while the temperature of H_2O only increased by nearly 1°C under the same conditions. Also, a concentration-dependent temperature increase for PM@HMSNs-DOX aqueous solutions was observed. Specially, the temperature of PM@HMSNs-DOX was much higher than the control, PDA, PDA@HMSNs-DOX, and

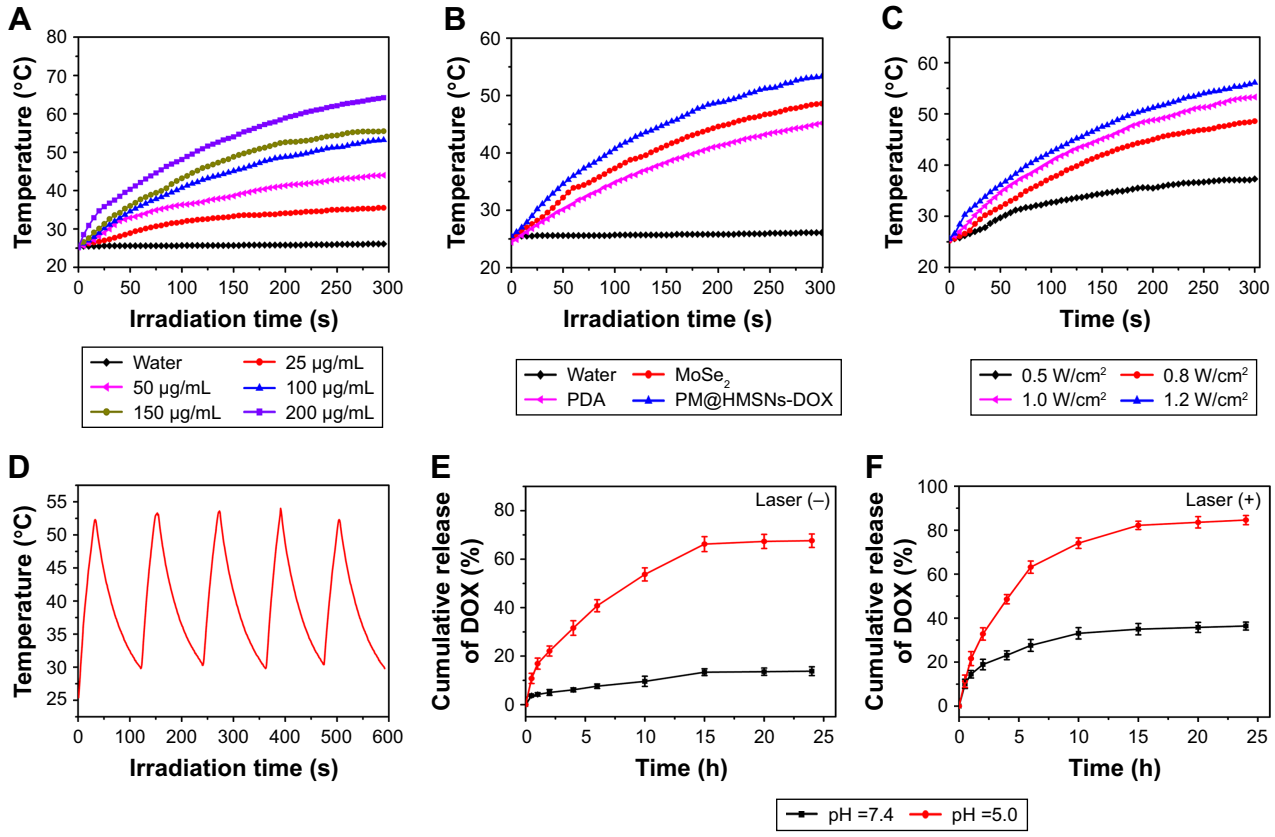

Figure 4 In vitro photothermal effect and stability of PM@HMSNs-DOX and drug release behavior at different pH values with or without NIR irradiation.
Notes: (**A**) Temperature change curves of PM@HMSNs-DOX aqueous solution with different concentrations (25–200 μg/mL) upon NIR laser irradiation (1 W/cm^2, 5 minutes). (**B**) Temperature change curves of water, PDA, $MoSe_2$, PDA@HMSNs-DOX, and PM@HMSNs-DOX. (**C**) Temperature change curves of PM@HMSNs-DOX aqueous solution with different power densities (0.5–1.2 W/cm^2, concentration: 100 μg/mL, 5 minutes). (**D**) Photothermal stability of PM@HMSNs-DOX within five cycles of NIR laser irradiation. (**E**) DOX release profiles from PM@HMSNs-DOX at different pH values (**E**) without and (**F**) with NIR laser irradiation.
Abbreviations: PM, polydopamine-coated $MoSe_2$; HMSNs, hollow mesoporous silica nanoparticles; DOX, doxorubicin; NIR, near-infrared; PDA, polydopamine.

$MoSe_2$, which evidenced the synergistic effect of PDA and $MoSe_2$ (Figure 4B). Meanwhile, the temperature increase of PM@HMSNs-DOX was dependent on the NIR laser power density (Figure 4C). More importantly, PM@HMSNs-DOX shows negligible change within five cycles of NIR laser on-off (Figure 4D). These results demonstrate that as-prepared PM@HMSNs-DOX could effectively convert NIR light into heat and could be used as an excellent photothermal agent. Meanwhile, the photothermal conversion efficiency of the synthesized PM@HMSNs-DOX was determined. It can be calculated to be 31.2% from the linear regression curve between the cooling stage and negative natural logarithm of driving force temperature of PM@HMSNs-DOX (Figure S3).

In vitro DOX release behavior

Subsequently, the cumulative release of DOX from PM@HMSNs-DOX was investigated by the dialysis method under different pH conditions with or without the 808 nm NIR laser irradiation. Firstly, the HMSNs-DOX-NH_2 showed an obvious burst release with >80% DOX release at pH 7.4 within 12 hours (Figure S4). In contrast, the cumulative drug release of DOX was only 13% in 24 hours at pH 7.4, indicating that $MoSe_2$@PDA could effectively block the pore of the HMSNs and prevent drug leakage (Figure 4E). Moreover, the release rate of DOX was much higher and the release amount of DOX reached 67% in 24 hours at pH 5.0. These results demonstrated that the boosted drug release at acidic pH is attributed to the breakage of PDA and the decrease of the electrostatic interaction between DOX and HMSNs.[43] Furthermore, it was found that the effective pH-responsive release manner could obviously facilitate the DOX released (Figure 4F). After laser irradiation, the release amount of DOX reached 84% at pH 5.0, which is much higher than that of 67% at the same condition but without laser irradiation, and also higher than that of 36.4% upon NIR laser irradiation in neutral condition. The NIR-triggered DOX release is mainly due to the heat generated by $MoSe_2$@PDA with laser irradiation, which can disrupt the interaction between DOX

and HMSNs and thus induce the release of DOX. Considering the more acidic environment in cancer cells (pH ~5.0), the coating of $MoSe_2$@PDA onto the HMSNs could possibly endow the nanoplatform with pH/NIR-responsive drug delivery capability, which is beneficial for cancer therapy.

In order to further understand the drug release behavior, the kinetics of drug release was assessed using some mathematical models. Coefficients of correlation (R^2) are used as an indicator of the best fitting. The linear regression values are shown in Table S1. The correlation coefficient values of Ritger–Peppas were found to be above 0.930 at different conditions, which indicated that DOX release was suitable to the models. It deserves to be mentioned that the k value increased with NIR irradiation and decrease in pH, indicating that the DOX release could be triggered by both NIR irradiation and pH. In addition, all the release exponents (n) were fitted <0.45, indicating that the DOX release kinetics corresponds to a Fickian diffusion mechanism. Based on this, the drug release kinetics further certified the pH/NIR-triggered DOX release behavior.

In vitro cellular uptake

Encouraged by the NIR-responsive drug release property of PM@HMSNs-DOX, cellular internalization and intracellular drug release were evaluated on MDA-MB-231 cells by CLSM. As depicted in Figure 5A, only sporadic red fluorescence was observed for the cells treated with free DOX. For cells treated with PM@HMSNs-DOX at the same DOX concentration, DOX was released from the nanoplatform once PM@HMSNs-DOX entered the cells, resulting in a much stronger red fluorescence measured in both the cytoplasm and nuclei. Meanwhile, the most remarkable red fluorescence signal was observed for cells treated with PM@HMSNs-DOX under NIR laser irradiation, demonstrating a higher uptake of PM@HMSNs-DOX mainly because the heating produced by the laser not only greatly promoted DOX release, but also enhanced the cellular uptake of PM@HMSNs-DOX.[44] Then, the intracellular fluorescence intensity was quantified by flow cytometry. The results confirmed strong DOX fluorescence in MDA-MB-231 cells incubated with PM@HMSNs-DOX, while cells treated with free DOX showed negligible fluorescence because of the lower cellular uptake of free DOX (Figure 5B and C). Besides, it could be observed that the fluorescence intensities of cells treated with PM@HMSNs-DOX under laser irradiation exhibited an increase of 1.87-fold than that without laser irradiation. Furthermore, ICP-AES was employed to quantify the amount of Si element in cells. In the laser irradiation group, the

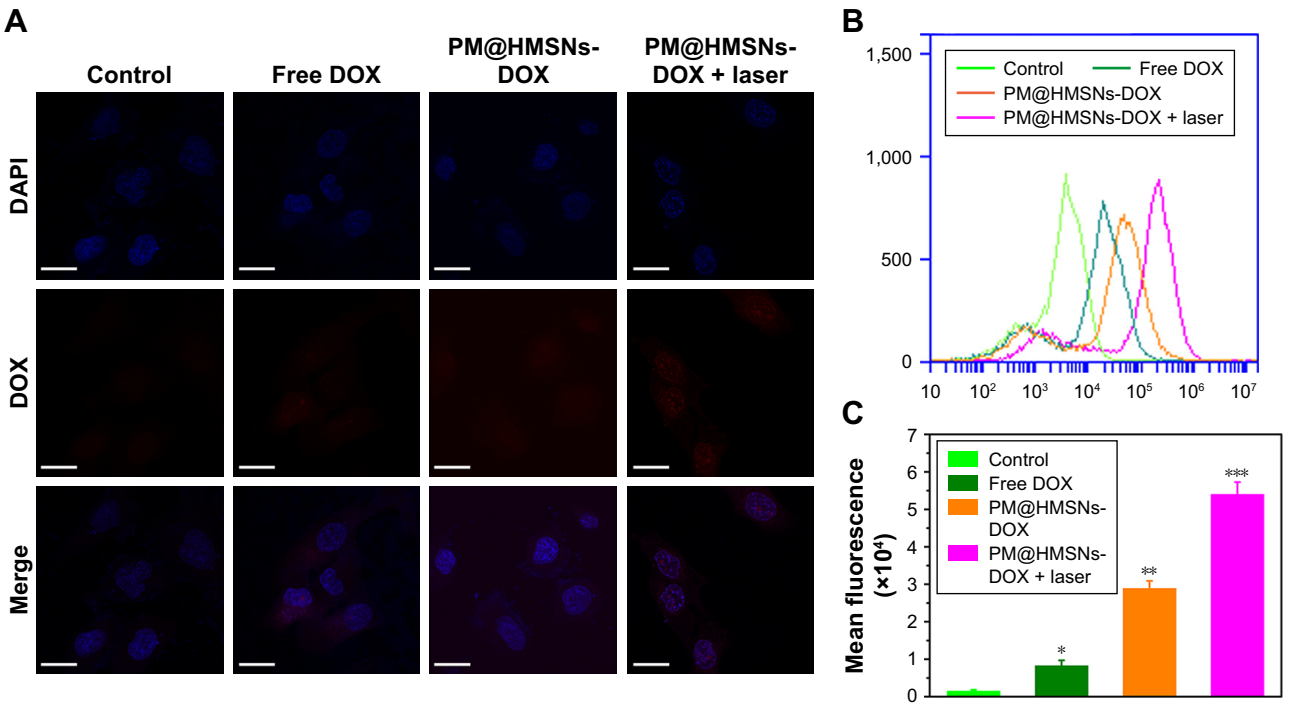

Figure 5 In vitro cellular uptake of PM@HMSNs-DOX.

Notes: (**A**) CLSM images of MDA-MB-231 cells incubated with fresh medium, free DOX, PM@HMSNs-DOX, and PM@HMSNs-DOX with laser irradiation for 4 hours (DOX concentration: 5 μg/mL). Scale bar: 50 μm. (**B**) Flow cytometry analyses of MDA-MB-231 cells incubated with fresh medium, free DOX, PM@HMSNs-DOX, and PM@HMSNs-DOX with laser irradiation for 4 hours. (**C**) The corresponding mean fluorescence intensity of MDA-MB-231 cells incubated with fresh medium, free DOX, PM@HMSNs-DOX, and PM@HMSNs-DOX with laser irradiation for 4 hours. *P<0.05, **P<0.01, and ***P<0.001.

Abbreviations: PM, polydopamine-coated $MoSe_2$; HMSNs, hollow mesoporous silica nanoparticles; DOX, doxorubicin; CLSM, confocal laser scanning; microscopy.

content of Si was 50 times that of the control group, and also about 2-fold of that in PM@HMSNs-DOX without laser irradiation (Figure S5). These results indicated that mild hyperthermia can significantly improve the endocytosis of PM@HMSNs-DOX.

In vitro cytotoxicity

The in vitro cytotoxicity of the nanoplatform against MDA-MB-231 cells was investigated by the CCK-8 assay. Without loading DOX, the PM@HMSNs possessed negligible cytotoxicity even at concentrations up to 500 μg/mL, indicating that PM@HMSNs have good biocompatibility (Figure S6). Upon drug loading, the combined effect of PTT and chemotherapy was investigated. MDA-MB-231 cells were incubated with various concentrations of PM@HMSNs-DOX at a series of DOX concentrations with or without laser irradiation. As shown in Figure 6A, comparing with DOX, PM@HMSNs-DOX demonstrated high inhibition against tumor cells, which is in accordance with the CLSM observations. Besides, with increasing drug concentrations, PM@HMSNs-DOX, PDA@HMSNs-DOX, and free DOX exhibited enhanced therapeutic effects on MDA-MB-231 cells, suggesting a concentration-dependent cytotoxic effect. Moreover, after NIR laser irradiation, the cytotoxicity increased dramatically with a cell viability of 16.5% at the DOX concentration of 15 μg/mL. Moreover, PM@HMSNs under NIR irradiation exhibited a relatively low cytotoxicity compared with PM@HMSNs-DOX plus NIR irradiation due to the absence of DOX (Figure S7). This result may be attributed to the excellent photothermal effect and improved mild hyperthermia-triggered drug release. Furthermore, live/dead cell assay was performed to visualize the anticancer efficacy (Figure 6B). It can be observed that almost all cells remained alive in the control group, showing the green fluorescence of calcein AM staining. As expected, more cancer cells were killed by PM@HMSNs-DOX with NIR laser irradiation. Compared with the cells that were treated with free DOX or not exposed to NIR, significant red fluorescence (dead cells) was observed. These results indicate the optimal synergistic therapeutic effect of PM@HMSNs-DOX upon NIR irradiation, which is consistent with that of the in vitro CCK-8 results. Overall, the as-prepared multifunctional nanoplatform can be efficiently used in the chemo-photothermal synergistic therapy of tumors.

In vivo antitumor effects

The above results demonstrated that the pH/NIR-responsive nanoplatform is promising for tumor chemo-PTT at the cellular level. Then, the in vivo antitumor study was carried out to demonstrate the combination therapy of PM@HMSNs-DOX on MDA-MB-231 tumor bearing mice. The tumor sizes and body weights of the treated mice were recorded after the various treatments were measured every 2 days within 2 weeks. As presented by the relative tumor volume (Figure 7A), tumors in the saline group increased rapidly during the process of treatment. By contrast, mice treated with PM@HMSNs-DOX and free DOX showed partially suppressed tumor effect. Also, the tumor growth in the PM@HMSNs-treated mice with laser irradiation was inhibited to some extent. This could be attributed to the

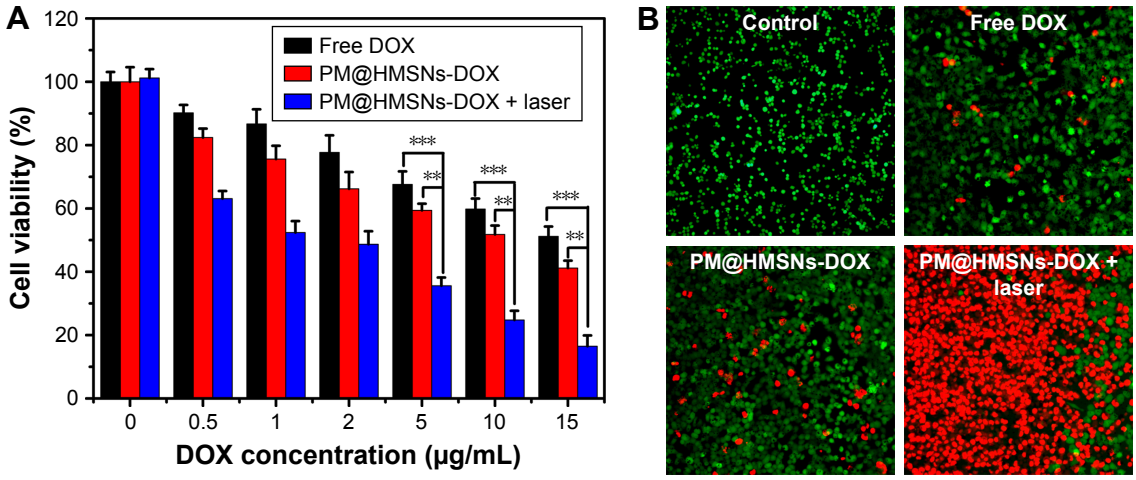

Figure 6 In vitro cytotoxicity study and calcein AM/PI staining analysis.

Notes: (**A**) Relative viabilities of MDA-MB-231 cells treated with free DOX, PM@HMSNs-DOX, PDA@HMSNs-DOX, and PM@HMSNs-DOX with irradiation by 808 nm laser. $^{**}P<0.01$, $^{***}P<0.001$. (**B**) Fluorescence images of calcein AM/PI-stained MDA-MB-231 cells incubated with fresh medium, control + laser, free DOX, PM@HMSNs-DOX, PDA@HMSNs-DOX, and PM@HMSNs-DOX with 808 nm laser irradiation, followed by 24 hours incubation with fresh medium.

Abbreviations: calcein AM, calcein acetoxymethyl ester; PI, propidium iodide; PM, polydopamine-coated $MoSe_2$; HMSNs, hollow mesoporous silica nanoparticles; DOX, doxorubicin; PDA, polydopamine.

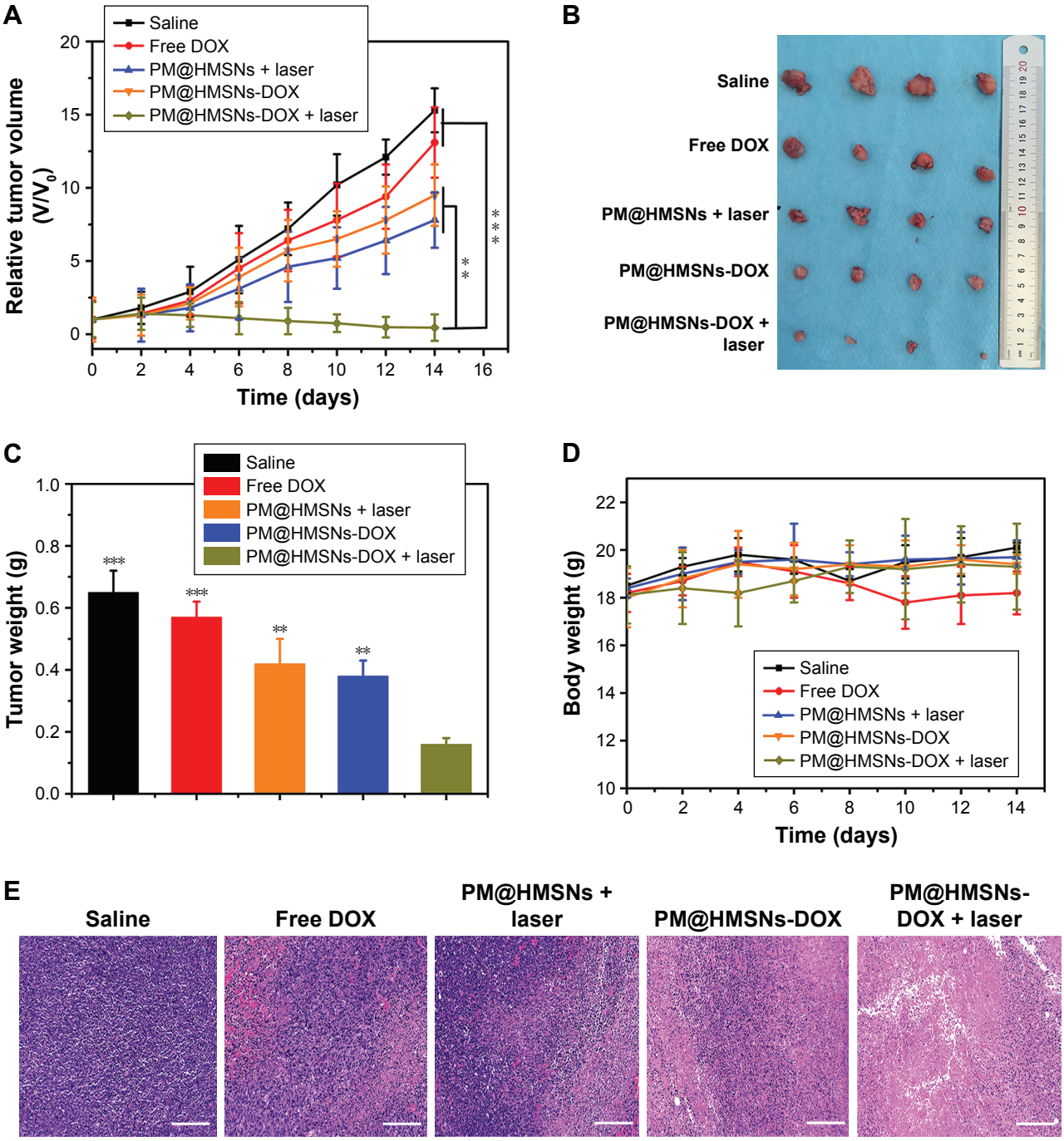

Figure 7 In vivo antitumor effect of MDA-MB-231 tumor bearing nude mice after intravenous injection of saline, free DOX, PM@HMSNs + laser, PDA@HMSNs-DOX + laser, PM@HMSNs-DOX with or without laser irradiation at an equivalent dose of DOX (7.5 mg/kg).

Notes: (**A**) Relative tumor volume after different treatments. (**B**) Representative photographs of the tumors collected from varying groups of mice at the end of the treatments (day 14). (**C**) The tumor weights at the end of therapy on day 14. (**D**) The body weight of mice during treatment. (**E**) Representative H&E staining in histologic images from the tumor tissues. $^{**}P<0.01$ and $^{***}P<0.001$. Scale bar: 50 μm.

Abbreviations: PM, polydopamine-coated $MoSe_2$; HMSNs, hollow mesoporous silica nanoparticles; DOX, doxorubicin; PDA, polydopamine.

limited effectiveness of single chemotherapy. A significant therapeutic effect is obtained in the cases of PDA@HMSNs-DOX with irradiation. Notably, the antitumor effect of PM@HMSNs-DOX upon NIR irradiation was superior to that in any other group. Outstanding tumor regression was observed with a relative tumor volume value of 0.45 on the 14th day, demonstrating the remarkably enhanced in vivo synergistic chemo-photothermal therapeutic efficiency. The harvested tumors from the sacrificial mice were administered and weighed (Figure 7B and C), the result clearly indicated that

the tumor size treated with PM@HMSNs-DOX upon NIR irradiation is significantly smaller than the other groups. These results demonstrated that combining chemotherapy with PTT was much more effective than PTT or chemotherapy alone. Furthermore, no significant body weight loss was observed in all groups during treatments, indicating less obvious side effects (Figure 7D).

In vivo histological analysis

To further verify the therapeutic effect, the different treatments on tumors were evaluated by H&E staining (Figure 7E). As expected, obvious necrotic regions can be observed in tumor tissues from the PM@HMSNs-DOX upon NIR irradiation groups, while the control groups show slight necrosis, indicating high efficiency in suppressing tumor growth of the synergistic effect of chemo-PTT. Moreover, the H&E analysis of major organs (heart, liver, spleen, lung, and kidney) (Figure 8A) shows no significant tissue damage in PBS and PM@HMSNs-DOX-treated group, confirming satisfactory safety of the designed nanosystem used in in vivo application.

In vivo pharmacokinetics and biodistribution analysis

Pharmacokinetic study was performed using SD rats. Free DOX and PM@HMSNs-DOX were intravenously administrated at an equivalent DOX dose of 10 mg/kg. Blood samples were collected at different time intervals

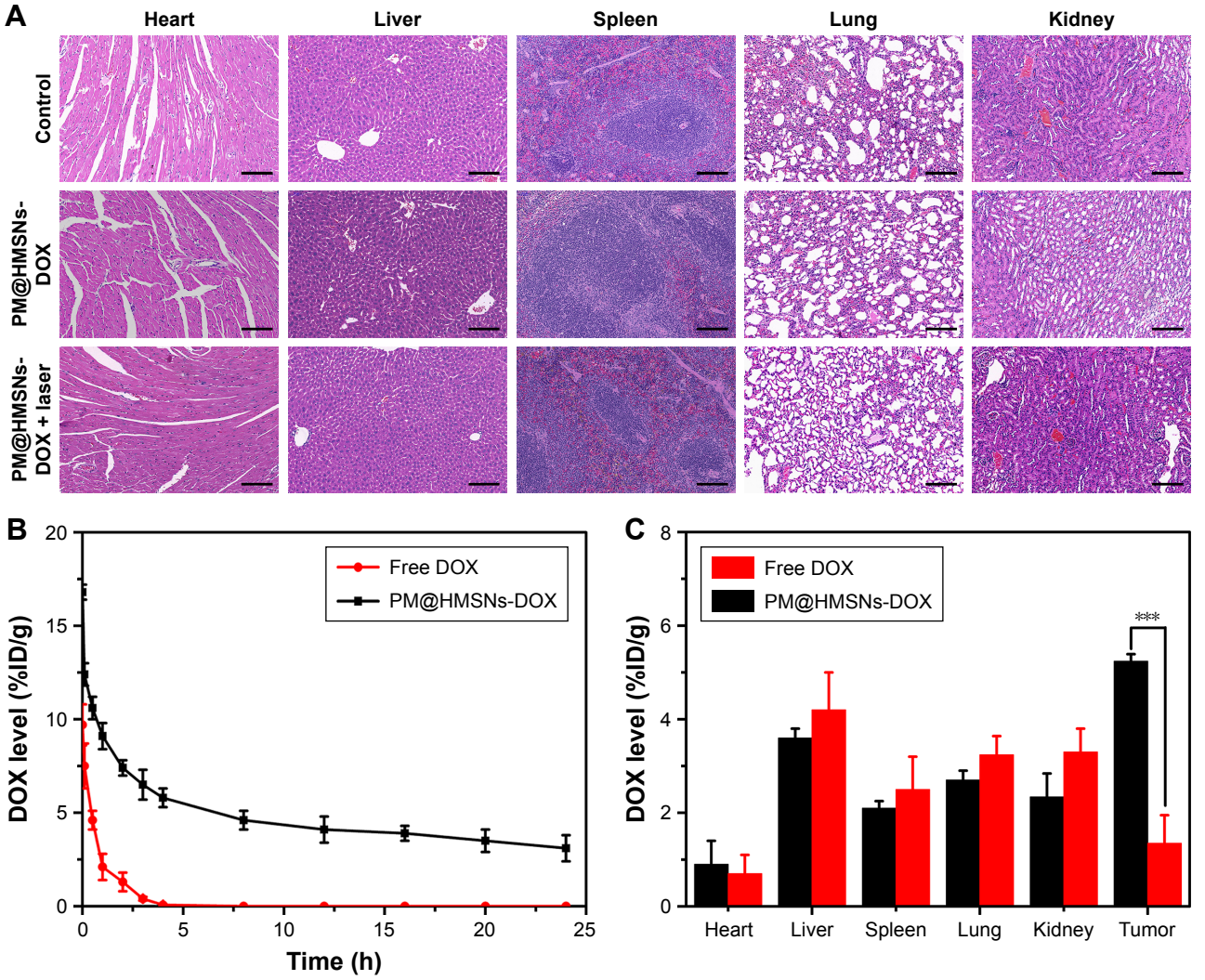

Figure 8 In vivo histology, pharmacokinetics, and biodistribution analysis.
Notes: (**A**) Representative tissue sections of mice stained with H&E after different treatments. Scale bar: 50 μm. (**B**) In vivo pharmacokinetics of PM@HMSNs-DOX and free DOX in mice. (**C**) Quantification of DOX accumulated in different organs and tumor using fluorescence spectroscopy. DOX uptake is expressed as injected dose per gram of tissue (%ID/g). Data are presented as mean ± standard deviation (n=3). ***$P<0.001$.
Abbreviations: PM, polydopamine-coated $MoSe_2$; HMSNs, hollow mesoporous silica nanoparticles; DOX, doxorubicin.

after injection and the plasma levels of DOX were determined by fluorescence spectroscopy to obtain the detailed pharmacokinetic profiles (Figure 8B). Notably, PM@HMSNs-DOX exhibited significantly prolonged blood circulation than free DOX. Free DOX was quickly cleared from blood, while a considerable amount of DOX was still detected in the blood even at the 24-hour injection of PM@HMSNs-DOX. These observations demonstrated that PM@HMSNs-DOX could prolong blood circulation time, leading to high tumor accumulation of DOX.

Next, the biodistribution of PM@HMSNs-DOX in tumor bearing mice was investigated after intravenous injection. The mice were sacrificed at 24 hours postinjection for extraction of heart, liver, spleen, lung, kidney, and tumor, followed by the measurement of DOX fluorescence in these tissues. As shown in Figure 8C, PM@HMSNs-DOX displayed a remarkably high DOX level of 5.24 %ID/g in the tumor, which was over 4-fold higher than that of the free DOX group. Moreover, PM@HMSNs-DOX displayed high accumulation in the liver, spleen, and lung, which may be attributed to the clearance effect by the reticuloendothelial system located in these organs.[45] These results demonstrated the long blood circulation time and enhanced permeability and retention effect of the nanoparticles at the tumor site.

Conclusion

We developed a multifunctional nanoplatform, PM@HMSNs-DOX, for the sustained and controlled delivery of DOX and chemo-PTT. In this design, HMSNs as a drug carrier exhibit a high drug loading capacity of 470 mg/g and pH-responsive DOX release behavior, which can be enhanced by laser irradiation. Then, the PDA-coated $MoSe_2$ layer was used as a gatekeeper to cap on the surface of the nanoparticle to realize excellent photothermal property. In vitro and in vivo experiments showed that PM@HMSNs-DOX upon NIR irradiation had enhanced therapeutic effects and superior tumor inhibiting effect by virtue of the synergistic chemo-PTT effect while the nanoplatform was biocompatible and essentially nontoxic. The dual-responsive nanoplatform was fabricated to not only take advantage of chemotherapy and PTT, but also integrate different photothermal agents to achieve synergistic photothermal ablation, which is a promising nanoplatform for therapeutic applications.

Acknowledgment

This study was supported by the Scientific Research and Innovation Team Funding Plan of Shanghai Sanda University.

Disclosure

The authors report no conflicts of interest in this work.

References

1. Shi J, Kantoff PW, Wooster R, Farokhzad OC. Cancer nanomedicine: progress, challenges and opportunities. *Nat Rev Cancer*. 2017;17(1):20–37.
2. Miller KD, Siegel RL, Lin CC, et al. Cancer treatment and survivorship statistics, 2016. *CA Cancer J Clin*. 2016;66(4):271–289.
3. Mcguire S, Report WC. World Cancer Report 2014. Geneva, Switzerland: World Health Organization, International Agency for Research on Cancer, WHO Press, 2015. *Adv Nutr*. 2016;7(2):418–419.
4. Veiseh O, Kievit FM, Ellenbogen RG, Zhang M. Cancer cell invasion: treatment and monitoring opportunities in nanomedicine. *Adv Drug Deliv Rev*. 2011;63(8):582–596.
5. Fan W, Yung B, Huang P, Chen X. Nanotechnology for Multimodal Synergistic Cancer Therapy. *Chem Rev*. 2017;117(22):13566–13638.
6. Dai Y, Xu C, Sun X, Chen X. Nanoparticle design strategies for enhanced anticancer therapy by exploiting the tumour microenvironment. *Chem Soc Rev*. 2017;46(12):3830–3852.
7. Jin R, Liu Z, Bai Y, Zhou Y, Gooding JJ, Chen X. Core-satellite mesoporous silica-gold nanotheranostics for biological stimuli triggered multimodal cancer therapy. *Adv Funct Mater*. 2018;28(31):1801961–1801970.
8. Lu N, Huang P, Fan W, et al. Tri-stimuli-responsive biodegradable theranostics for mild hyperthermia enhanced chemotherapy. *Biomaterials*. 2017;126:39–48.
9. Dong Z, Feng L, Zhu W, et al. $CaCO_3$ nanoparticles as an ultra-sensitive tumor-pH-responsive nanoplatform enabling real-time drug release monitoring and cancer combination therapy. *Biomaterials*. 2016;110:60–70.
10. Liu J, Yang G, Zhu W, et al. Light-controlled drug release from singlet-oxygen sensitive nanoscale coordination polymers enabling cancer combination therapy. *Biomaterials*. 2017;146:40–48.
11. Zheng DW, Chen JL, Zhu JY, et al. Highly integrated nano-platform for breaking the barrier between chemotherapy and immunotherapy. *Nano Lett*. 2016;16(7):4341–4347.
12. Liu Y, Zhen W, Jin L, et al. All-in-one theranostic nanoagent with enhanced reactive oxygen species generation and modulating tumor microenvironment ability for effective tumor eradication. *ACS Nano*. 2018;12(5):4886–4893.
13. Chen Q, Feng L, Liu J, et al. Intelligent albumin-MnO_2 nanoparticles as pH-/H_2O_2-responsive dissociable nanocarriers to modulate tumor hypoxia for effective combination therapy. *Adv Mater*. 2016;28(33):7129–7136.
14. Cai Y, Liang P, Tang Q, et al. Diketopyrrolopyrrole-triphenylamine organic nanoparticles as multifunctional reagents for photoacoustic imaging-guided photodynamic/photothermal synergistic tumor therapy. *ACS Nano*. 2017;11(1):1054–1063.
15. Chen YW, Su YL, Hu SH, Chen SY, Yl S, Sh H. Functionalized graphene nanocomposites for enhancing photothermal therapy in tumor treatment. *Adv Drug Deliv Rev*. 2016;105(Pt B):190–204.
16. Mekaru H, Lu J, Tamanoi F. Development of mesoporous silica-based nanoparticles with controlled release capability for cancer therapy. *Adv Drug Deliv Rev*. 2015;95:40–49.
17. Yang Y, Zhu W, Dong Z, et al. 1D coordination polymer nanofibers for low-temperature photothermal therapy. *Adv Mater*. 2017;29(40):1703588.
18. Wu SH, Mou CY, Lin HP. Synthesis of mesoporous silica nanoparticles. *Chem Soc Rev*. 2013;42(9):3862–3875.
19. Chen Y, Meng Q, Wu M, et al. Hollow mesoporous organosilica nanoparticles: a generic intelligent framework-hybridization approach for biomedicine. *J Am Chem Soc*. 2014;136(46):16326–16334.
20. Fang W, Tang S, Liu P, Fang X, Gong J, Zheng N. Pd nanosheet-covered hollow mesoporous silica nanoparticles as a platform for the chemo-photothermal treatment of cancer cells. *Small*. 2012;8(24):3816–3822.

21. Liu X, Fu F, Xu K, et al. Folic acid-conjugated hollow mesoporous silica/CuS nanocomposites as a difunctional nanoplatform for targeted chemo-photothermal therapy of cancer cells. *J Mater Chem B*. 2014; 2(33):5358–5367.
22. Luo L, Bian Y, Liu Y, et al. Combined near infrared photothermal therapy and chemotherapy using gold nanoshells coated liposomes to enhance antitumor effect. *Small*. 2016;12(30):4103–4112.
23. Chen D, Dougherty CA, Zhu K, Hong H. Theranostic applications of carbon nanomaterials in cancer: Focus on imaging and cargo delivery. *J Control Release*. 2015;210:230–245.
24. Tao W, Zhu X, Yu X, et al. Black phosphorus nanosheets as a robust delivery platform for cancer theranostics. *Adv Mater*. 2017;29(1): 1603276.
25. Liang G, Jin X, Qin H, Xing D. Glutathione-capped, renal-clearable CuS nanodots for photoacoustic imaging and photothermal therapy. *J Mater Chem B*. 2017;5(31):6366–6375.
26. Sheng D, Liu T, Deng L, et al. Perfluorooctyl bromide & indocyanine green co-loaded nanoliposomes for enhanced multimodal imaging-guided phototherapy. *Biomaterials*. 2018;165:1–13.
27. Zhong X, Yang K, Dong Z, et al. Polydopamine as a biocompatible multifunctional nanocarrier for combined radioisotope therapy and chemotherapy of cancer. *Adv Funct Mater*. 2015;25(47):7327–7336.
28. Xu Y, Wang X, Zhang WL, Lv F, Guo S. Recent progress in two-dimensional inorganic quantum dots. *Chem Soc Rev*. 2018;47(2): 586–625.
29. Song X, Hu J, Zeng H. Two-dimensional semiconductors: recent progress and future perspectives. *J Mater Chem C*. 2013;1(17):2952–2969.
30. Li X, Shan J, Zhang W, Su S, Yuwen L, Wang L. Recent advances in synthesis and biomedical applications of two-dimensional transition metal dichalcogenide nanosheets. *Small*. 2017;13(5):1602660.
31. Zhao W, Li A, Chen C, et al. Transferrin-decorated, MoS_2-capped hollow mesoporous silica nanospheres as a self-guided chemo–photothermal nanoplatform for controlled drug release and thermotherapy. *J Mater Chem B*. 2017;5(35):7403–7414.
32. Wu J, Bremner DH, Niu S, et al. Functionalized MoS_2 nanosheet-capped periodic mesoporous organosilicas as a multifunctional platform for synergistic targeted chemo-photothermal therapy. *Chem Eng J*. 2018; 342:90–102.
33. Chen Y, Ai K, Liu J, Ren X, Jiang C, Lu L. Polydopamine-based coordination nanocomplex for T_1/T_2 dual mode magnetic resonance imaging-guided chemo-photothermal synergistic therapy. *Biomaterials*. 2016;77:198–206.
34. Chang D, Gao Y, Wang L, et al. Polydopamine-based surface modification of mesoporous silica nanoparticles as pH-sensitive drug delivery vehicles for cancer therapy. *J Colloid Interface Sci*. 2016;463: 279–287.
35. Shao L, Zhang R, Lu J, Zhao C, Deng X, Wu Y. Mesoporous silica coated polydopamine functionalized reduced graphene oxide for synergistic targeted chemo-photothermal therapy. *ACS Appl Mater Interfaces*. 2017;9(2):1226–1236.
36. Wong PT, Choi SK. Mechanisms of drug release in nanotherapeutic delivery systems. *Chem Rev*. 2015;115(9):3388–3432.
37. Chen Y, Chen H, Guo L, et al. Hollow/rattle-type mesoporous nanostructures by a structural difference-based selective etching strategy. *ACS Nano*. 2010;4(1):529–539.
38. Wang C, Bai J, Liu Y, Jia X, Jiang X. Polydopamine coated selenide molybdenum: a new photothermal nanocarrier for highly effective chemo-photothermal synergistic therapy. *ACS Biomater Sci Eng*. 2016; 2(11):2011–2017.
39. Feng W, Chen L, Qin M, et al. Flower-like PEGylated MoS_2 nanoflakes for near-infrared photothermal cancer therapy. *Sci Rep*. 2015;5: 17422–17435.
40. Zeng X, Liu G, Tao W, et al. A drug-self-gated mesoporous antitumor nanoplatform based on pH-sensitive dynamic covalent bond. *Adv Funct Mater*. 2017;27(11):1605985.
41. Croissant JG, Cattoën X, Wong MC, Durand JO, Khashab NM. Syntheses and applications of periodic mesoporous organosilica nanoparticles. *Nanoscale*. 2015;7(48):20318–20334.
42. Kim SH, In I, Park SY. pH-responsive NIR-absorbing fluorescent polydopamine with hyaluronic acid for dual targeting and synergistic effects of photothermal and chemotherapy. *Biomacromolecules*. 2017;18(6): 1825–1835.
43. Wang Y, Wang K, Zhao J, et al. Multifunctional mesoporous silica-coated graphene nanosheet used for chemo-photothermal synergistic targeted therapy of glioma. *J Am Chem Soc*. 2013;135(12):4799–4804.
44. Li C, Zhang Y, Li Z, et al. Light-Responsive Biodegradable Nanorattles for Cancer Theranostics. *Adv Mater*. 2018;30(8):1706150–1706158.
45. Yang K, Gong H, Shi X, Wan J, Zhang Y, Liu Z. In vivo biodistribution and toxicology of functionalized nano-graphene oxide in mice after oral and intraperitoneal administration. *Biomaterials*. 2013;34(11): 2787–2795.